AD-A159 587 ARCTIC OCEAN BACKGROUND NOISE CAUSED BY RIDGING OF SEA ICE(U) FLOW INDUSTRIES INC KENT WA R S PRITCHARD JUL 83 TR-266/07-83 N00014-82-C-0002 1/1

UNCLASSIFIED F/G 20/1 NL

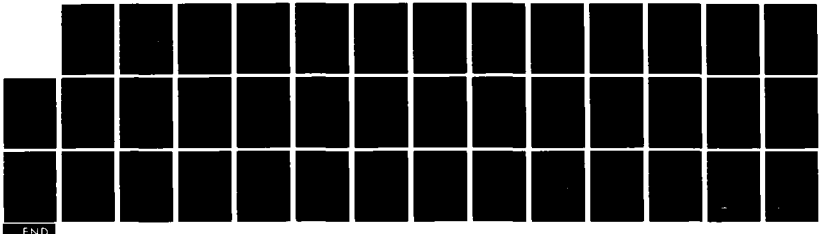

END

FILMED

DTIC

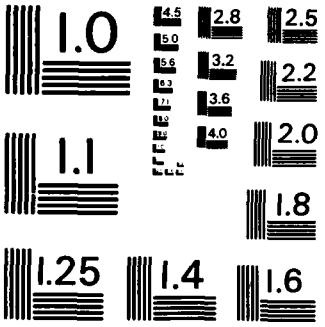

MICROCOPY RESOLUTION TEST CHART
NATIONAL BUREAU OF STANDARDS - 1963 - A

PHOTOGRAPH THIS SHEET

AD-A159 587

DTIC ACCESSION NUMBER

LEVEL

INVENTORY

TR-266/07-83

DOCUMENT IDENTIFICATION

July 1983

DISTRIBUTION STATEMENT

ACCESSION FOR	
NTIS GRA&I	☒
DTIC TAB	☐
UNANNOUNCED	☐
JUSTIFICATION	
BY	
DISTRIBUTION /	
AVAILABILITY CODES	
DIST	AVAIL AND/OR SPECIAL
A-1	

DISTRIBUTION STAMP

DATE ACCESSIONED

DATE RETURNED

85 10 02 127

DATE RECEIVED IN DTIC

REGISTERED OR CERTIFIED NO.

PHOTOGRAPH THIS SHEET AND RETURN TO DTIC-DDAC

DTIC FORM 70A DEC 83

DOCUMENT PROCESSING SHEET

PREVIOUS EDITION MAY BE USED UNTIL STOCK IS EXHAUSTED.

TR-266/07-83

ARCTIC OCEAN BACKGROUND NOISE CAUSED BY RIDGING OF SEA ICE

Robert S. Pritchard

July 1983

Flow Industries, Inc.
Research and Technology
21414 68th Avenue South
Kent, Washington 98032
(206) 872-8500
TWX: 910 447-2767

SECURITY CLASSIFICATION OF THIS PAGE

REPORT DOCUMENTATION PAGE

1a. REPORT SECURITY CLASSIFICATION UNCLASSIFIED	1b. RESTRICTIVE MARKINGS
2a. SECURITY CLASSIFICATION AUTHORITY N/A	3. DISTRIBUTION / AVAILABILITY OF REPORT
2b. DECLASSIFICATION / DOWNGRADING SCHEDULE N/A	UNLIMITED, APPROVED FOR PUBLIC RELEASE
4. PERFORMING ORGANIZATION REPORT NUMBER(S) TR-266107-83	5. MONITORING ORGANIZATION REPORT NUMBER(S)
6a. NAME OF PERFORMING ORGANIZATION FLOW INDUSTRIES, INC. — 6b. OFFICE SYMBOL (If applicable)	7a. NAME OF MONITORING ORGANIZATION OFFICE OF NAVAL RESEARCH
6c. ADDRESS (City, State, and ZIP Code) 21414 68th AVE. S. KENT, WA 98032	7b. ADDRESS (City, State, and ZIP Code) 800 N. QUINCY ST. ARLINGTON, VA 22217-5000
8a. NAME OF FUNDING / SPONSORING ORGANIZATION ONR — 8b. OFFICE SYMBOL (If applicable)	9. PROCUREMENT INSTRUMENT IDENTIFICATION NUMBER N00014-82-C-0002
8c. ADDRESS (City, State, and ZIP Code) 800 N. QUINCY ST. ARLINGTON, VA 22217-5000	10. SOURCE OF FUNDING NUMBERS PROGRAM ELEMENT NO.: 61153N — PROJECT NO.: RR03205 — TASK NO. — WORK UNIT ACCESSION NO.
11. TITLE (Include Security Classification) (U) ARCTIC OCEAN BACKGROUND NOISE CAUSED BY RIDGING OF SEA ICE	
12. PERSONAL AUTHOR(S) ROBERT S. PRITCHARD	
13a. TYPE OF REPORT FINAL — 13b. TIME COVERED FROM 1 OCT 81 TO 30 SEP 82	14. DATE OF REPORT (Year, Month, Day) JULY 1983 — 15. PAGE COUNT 36
16. SUPPLEMENTARY NOTATION	

17. COSATI CODES			18. SUBJECT TERMS (Continue on reverse if necessary and identify by block number)
FIELD	GROUP	SUB-GROUP	

19 ABSTRACT (Continue on reverse if necessary and identify by block number)

A new method is presented to explain how noise is generated under pack ice by ridging of the pack ice. The energy dissipated during the ridging process is assumed to be the proper measure of the noise source level. Noise source levels generated by ridging are simulated. Noise intensity at a specific site is calculated by summing signals from all these sources after accounting for propagation losses. Calculations are made to compare this simulated noise with observations for an experiment conducted during the winter of 1975-76 in the Beaufort Sea. During a 120-day period, 46% of the intensity of the noise signal is explained using this process, and over several 20-day periods, in excess of 64% is explained. In addition to explaining a significant amount of energy and ambient noise, the model is attractive on physical grounds and properly explains lack of noise when winds are high but ice is strong enough to resist ridging.

20. DISTRIBUTION / AVAILABILITY OF ABSTRACT ☒ UNCLASSIFIED/UNLIMITED ☐ SAME AS RPT. ☐ DTIC USERS	21. ABSTRACT SECURITY CLASSIFICATION UNCLASSIFIED
22a. NAME OF RESPONSIBLE INDIVIDUAL ROBERT OBROCHTA	22b. TELEPHONE (Include Area Code) 202-696-4720 — 22c. OFFICE SYMBOL

DD FORM 1473, 84 MAR — 83 APR edition may be used until exhausted. All other editions are obsolete.

SECURITY CLASSIFICATION OF THIS PAGE

UNCLASSIFIED

TR-266/07-83

ARCTIC OCEAN BACKGROUND NOISE CAUSED BY RIDGING OF SEA ICE

Robert S. Pritchard

July 1983

Flow Industries, Inc.
Research and Technology
21414 68th Avenue South
Kent, Washington 98032
(206) 872-8500
TWX: 910 447-2762

Robert S. Pritchard
Submitted to J. Acoust. Soc. Am.
102/03-83
TR-266/07-83

Arctic Ocean Background Noise Caused by Ridging of Sea Ice

by

Robert S. Pritchard

July 1983

Flow Industries, Inc.
Research and Technology
21414 - 68th Avenue South
Kent, Washington 98032

ABSTRACT

A new method is presented to explain how noise is generated under pack ice by ridging of the pack ice. The energy dissipated during the ridging process is assumed to be the proper measure of the noise source level. Noise source levels generated by ridging are simulated. Noise intensity at a specific site is calculated by summing signals from all these sources after accounting for propagation losses. Calculations are made to compare this simulated noise with observations for an experiment conducted during the winter of 1975-76 in the Beaufort Sea. During a 120-day period, 46% of the intensity of the noise signal is explained using this process, and over several 20-day periods, in excess of 64% is explained. In addition to explaining a significant amount of energy and ambient noise, the model is attractive on physical grounds and properly explains lack of noise when winds are high but ice is strong enough to resist ridging.

INTRODUCTION

As a sea ice cover moves, fractures and deforms it generates noise which, in combination with other background noise, interferes with sonar, communica- tions and weapons control signals. Background noise under sea ice has been measured under a wide variety of conditions. Although various investi- have studied the characteristics of this noise (see Ref. 1 for review), little work has been done to relate the observed noise to specific processes. The work that has been done includes attempts to relate background noise level under sea ice to wind speed, changes in air temperature, cracking of the ice and stresses and strains in the ice. Separate correlations of ambient noise with wind speed, ice stresses and ice strains have shown that each could account for some but not all of the observed noise.

noise.[2,3,4] Better correlations have been achieved by relating thermal cracking due to daily temperature drops[5,6] and stress-induced microcracking. These initial attempts to relate a single noise-making process to ambient noise signals can result in a better understanding of and the potential for modeling noise under sea ice.

The single largest source of noise in the Arctic in the winter is thought to be ridging. In this paper, we examine the relationship between observed low-frequency background noise and the occurrence of ridging, as simulated by an ice model. Thus, while concentrating on a single noise-producing process, we can attempt to explain a significant amount of the background noise.

The critical assumption made in this work is that, in ridging, the intensity of a noise signal at its source (the ridge) is related to the amount of energy dissipated in the ridging process. A phenomenological comparison is made in which a theoretical estimate of noise due to ridging is compared with observed noise at a site in the central Beaufort Sea during the winter of 1975-76. The individual, small-scale noise-making processes that occur in ridging have not yet been studied. The present phenomenological study is felt to be a necessary preliminary effort in determining if a more detailed study would be fruitful.

In this study, a model is developed to estimate the noise intensity received at any site from ridging at all points on the ice cover. This relationship depends on the amount of energy dissipated due to noise production and accounts for transmission losses during propagation. The model is applied to the Beaufort Sea during the AIDJEX[7] main experiment (winter 1975-76) when background noise observations are available. A special method for simulating ridging is developed to use the ice motion data obtained from the manned camp

and buoys deployed during that time. Data limitations restrict our study to one-third octave bands centered around 10 Hz and 32 Hz. However, the theory can be extended to include a wider range of frequencies. Comparisons are made to estimate the fraction of total variance of observed noise that can be explained by this model. Error estimates are provided to show that the unexplained variance can be attributed to data limitations and that the basic hypothesis of the theory remains plausible. As a result, it is suggested that further work is justified.

I. NOISE SIMULATION MODEL

The processes that create noise can occur everywhere in the sea ice cover. To describe the total observed noise at a specific site, the sound waves reaching that specific site from all of the locations at which noise is generated must be taken into account. The magnitude or intensity of the noise at its sources must, of course, be known, and it must be specified everywhere. Practically, then, a model must relate the noise source level to some measurable variable that can be determined from knowledge of ice conditions, wind, current, temperature and other environmental parameters. Finally, as the acoustic waves propagate toward the observation site, they are dispersed and attenuated geometrically by reflection off the sea floor and the underside of the ice cover and by sound speed gradients. The approach presented here attempts to account for all of these factors, thereby providing a mathematical model formulated on basic physical principles of acoustics.

Many different processes occur that generate noise. The types of processes and the relative importance of their contributions to the total observed noise vary by both season and location. This work concentrates on wintertime

the central Beaufort Sea. In these heavy ice conditions, ridging is generally believed to be the single largest noise source. But even though ridging is often thought of as one large-scale geophysical process, it is in fact a combination of many small-scale processes. During ridge building, sea ice is fractured in bending, ice floes slide against one another to be crushed and sheared, and the resultant blocks are piled up and down against gravitational attraction.

A. Geophysical-scale model

Sea ice dynamics understanding has increased immeasurably in recent years, and, fortunately, the capability to simulate sea ice behavior has kept pace. Extensions to the AIDJEX model,[8] on which the present work is based, have been reported in Ref. 9. Of these extensions, the relationship developed to estimate the mechanical energy budget of the ice cover[10] is the most critical for this work. Here it is hypothesized that energy dissipated by large-scale failure processes such as ridging is the proper measure of energy available for conversion into acoustic signals. Thus, the capability to estimate these dissipation terms is necessary to the success of the present work. More detailed results on these modeling capabilities have been presented elsewhere[11] and estimates have been made of the Beaufort Sea energy budget during AIDJEX.[12]

The small-scale mechanisms in ridging dissipate energy that provides energy sources for acoustic signals. If these small-scale mechanism energy sinks are to be useful for explaining ambient noise, there must be a way to measure them at different times and locations. Fortunately, the AIDJEX model

does provide a way to calculate these energy sinks in terms of the geophysical-scale behavior. Specifically, in a constitutive law, it is assumed that the energy dissipated by the geophysical-scale stress during deformations is equal to the energy dissipated by these small-scale mechanisms. In the model, expressions are available to estimate these energy dissipation levels as a function of ice conditions at different times and locations.

The large-scale constitutive behavior is represented by an elastic-plastic mathematical model. As in other plasticity models, the stress is limited to lie within a yield surface. However, a stress resultant $\underset{\sim}{\sigma}$ is used. This stress resultant is the Cauchy stress integrated through the ice thickness. The theory is two-dimensional.

An isotropic, diamond-shaped yield surface is used in our computations. The yield criterion is given by

$$\phi(\sigma_I, \sigma_{II}) \leq 0 \tag{1}$$

where $\sigma_I = \frac{1}{2} \operatorname{tr} \underset{\sim}{\sigma}$ and $\sigma_{II} = \frac{1}{2} \operatorname{tr} \underset{\sim}{\sigma}' \underset{\sim}{\sigma}'^{1/2}$, with $\underset{\sim}{\sigma}' = \underset{\sim}{\sigma} - \sigma_I \underset{\sim}{1}$. The invariants σ_I and σ_{II} are half the sum and difference of the principal stress value, respectively, and p* is the ice strength in isotropic compression. The shear stress invariant σ_{II} is nonnegative when defined in this way. Plastic deformations are assumed to satisfy an associated flow rule. Thus, the plastic stretching $\underset{\sim}{D}_p$ is orthogonal to the yield surface and may be expressed as

$$\underset{\sim}{D}_p = \lambda \frac{\partial \phi}{\partial \underset{\sim}{\sigma}} \tag{2}$$

where λ is a nonnegative scalar.

A linear elastic law is assumed when stress is within the yield surface

$$\underset{\sim}{\sigma} = (M_1 \quad M_2) \underset{\sim}{1} \operatorname{tr} \underset{\sim}{e} + 2 M_2 \underset{\sim}{e} \tag{3}$$

where $\underset{\sim}{e}$ is elastic strain, and M_1 and M_2 are the bulk and shear moduli, respectively. The elastic strain is related to stretching, $\underset{\sim}{D}$, spin, $\underset{\sim}{W}$, and plastic stretching by the relationship[13]

$$\dot{\underset{\sim}{e}} - \underset{\sim}{We} + \underset{\sim}{eW} = \underset{\sim}{D} - \underset{\sim}{D}_p \quad . \tag{4}$$

Ice strength is determined as a function of the ice thickness distribution. Changes in the strength occur as deformations change the thickness distribution, which is governed by the relationship

$$\dot{G} + f_t \frac{\partial G}{\partial h} = \psi - G\underset{\sim}{\nabla}\cdot\underset{\sim}{v} \tag{5}$$

where G(h,t) is the fraction of area covered by ice thinner than h at time t, and ψ is the rate of ice production of ice thinner than h due to mechanical redistribution.[14] Assuming ψ is linear in the rate of plastic stretching, then

$$\psi = D_p[\alpha_o(\theta) + \alpha_r(\theta)W_r] \quad . \tag{6}$$

Here, $D_p = \left[(D_p)_I^2 + (D_p)_{II}^2\right]^{1/2}$ where $(D_p)_I$ and $(D_p)_{II}$ are the sum and difference of principal stretching values. The angle $\theta = \arctan\left[(D_p)_{II}/(D_p)_I\right]$ is the ratio of shearing to dilating. The coefficient α_o is the fraction of open water created by a unit of deformation. Conservation of mass requires α_o and α_r to be related by $\alpha_o - \alpha_r = \cos\theta$. The variable W_r describes the conversion of thin ice into thicker ice by ridging and is a complicated functional of the thickness distribution.

The rate at which energy is dissipated by large-scale stresses during deformation is determined as the product of stress and permanent stretching. This is the dissipative stress power, $p_\ell = \mathrm{tr}\,\underset{\sim}{\sigma}\,\underset{\sim}{D}_p$. This large-scale measure of

nergy dissipation is equated to the sum of identifiable small-scale energy inks. Thus,

$$P_\ell = \sum_\alpha q_\alpha \tag{7}$$

here q_α is the set of small-scale energy sinks that are known to dissipate echanical energy. This relationship provides an estimate of the large-scale ice strength and helps relate the redistribution function to the constitutive law. For this study of noise sources, the relationship also provides a means of estimating the magnitude of the noise source level. We assume that each small-scale energy sink is a source of noise and that the energy dissipated by each sink can be determined from the large-scale energy dissipated.

Gravitational potential energy changes and dissipation by friction as ice blocks slide through the keel and sail are considered to determine the force needed to build a ridge.[15] This concept has been generalized by allowing both compression and shear.[16] The change in gravitational potential energy, q_p, as ice is piled up and down into the ridge sail and keel is given by

$$q_p = c_p \int_0^\infty h^2 \frac{\partial \psi}{\partial h} \, dl \tag{8}$$

$$c_p = \frac{1}{2} \hat{\rho} g \tag{9}$$

s the gravitational acceleration, and

$$\hat{\rho} = \frac{\rho}{\rho_w} (\rho_w - \rho) \tag{10}$$

In concept, more buoys would allow better resolution and, thus, would reduce this potential error. However, the sea ice constitutive law assumes that many ridges are forming within a triangle to ensure isotropy and homogeneity, so 10 km is roughly the lower limit for achieving better resolution with a more dense buoy array. In addition, as buoys approach one another, the uncertainty in stretching from the velocity inhomogeneity variation becomes so large that it dominates errors. Therefore, triangles roughly on the order of 50 km provide data that are as accurate and consistent as is reasonable for using this simulation technique.

Another potential source of error is due to the assumed thickness distribution used in the simulations. The initial thickness distribution is reasonably accurate for Julian day 465. It is used, however, to begin the simulations for each 20-day block. This choice affects the strength level, which, if constant, would not affect the comparison, and it affects variations in strength due to redistribution. The effects of this assumption are not known. Our inability to measure the thickness distribution of sea ice is a problem with all simulations of sea ice behavior.

6. CONCLUSIONS

In this paper we have introduced a new concept to explain background noise under Arctic sea ice. The concept is based on the hypothesis that energy dissipated by the ice in ridge building is related to the intensity of the source level of background noise. A mathematical model of sea ice behavior is capable of simulating the energy dissipated by stress during deformation everywhere in the ice cover. The spatial distribution of noise sources may therefore be simulated at any time. If transmission losses are taken into

as a typical value for the time period used in our analysis. This uncertainty in the variation in velocity gives rise to uncertainties in stretching that are 0.7×10^{-7} s^{-1} at the 90% confidence level during spring. These errors assume a gauge length of 100 km. Smaller scale averages generate proportionately larger uncertainties in stretching. Since triangles are typically 50 km in size, uncertainties in stretching are on the order of 1.5×10^{-7} s^{-1}.

It is difficult, if not impossible, to estimate uncertainty in the power dissipated because the extremely large uncertainty in stretching makes uncertainty in stress unrealistically large. For a strength of 5×10^{4} N/m, the stretching uncertainty gives rise to an uncertainty of 7×10^{-3} W/m^2. If this is input as a constant error over a circular domain with a radius of 500 km and the transmission loss function, Eq. (22), is assumed, then integration gives an error in simulated noise of about 1×10^{9} W. This theoretical maximum error is as large as maximum simulated noise values (Figures 3 and 4). Another estimate of velocity inhomogeneity errors is obtained by looking at quiet times when all simulated noise may be assumed to be due to velocity inhomogeneities. These values were discussed earlier. Fortunately, the actual values are about 25% of the simulated maxima, far lower than the theoretical maxima.

Uncertainties in the transmission loss law also limit the accuracy of this simulation technique. First, the transmission loss law is an empirical fit to data, and some unexplained variance must by expected. Second, the transmission loss law decays exponentially from the source. Thus, any sources very near the observation location will be very sensitive to the location of the source. But a source can be located to only be within a specific triangle, rather than at an exact site within the triangle. This is a limitation of the basic approach [illegible] distance between buoy [illegible] is controlled by triangle [illegible]

Scatter plots of observed signals and simulated noise signals from q_r are given in Figures 5 and 6 for 10 and 32 Hz, respectively. These plots show that the observed and simulated signals tend to rise and fall together. Many signals occur at low noise levels, which causes a problem in the plots because the data points tend to black out the area. It would have been simple to plot data at logarithmic scales to spread out the points at low noise levels, but this would have emphasized data that are subject to relatively large errors. Several individual events appear in the scatter plots. These have been shown by connecting the dots to make a "spaghetti" plot. The path taken by the larger events clearly shows the correlation. Some difference appears, though, as individual events are related by different regression equations or slopes. This is probably caused by our lack of resolution (triangle size), by inaccuracies in the transmission loss law, or by our uncertainty in ice conditions and therefore ice strength during the experiment.

The data are obviously shifted to the right and do not pass through the origin. This is caused by excessive energy being dissipated as individual buoys respond to small-scale velocity inhomogeneities that are not modeled by the sea ice constitutive law. If the ridging process were modeled perfectly, one would expect the regression line to intersect the ordinate and not the abscissa, because other noise-making processes would generate noise that has not been modeled here.

Although errors can occur because spatial variations in the velocity field are not smooth, the large-scale average is a reasonable estimate of the deformations occurring within the triangle. The inhomogeneity variation has been estimated to be on the order of 0.4 cm/s during spring 1975.[22] We use this

the comparison varies throughout the 4-month period. In addition, three energy dissipation variables are compared with observed noise to determine which one explains the most variance in observed noise. For the entire period, the energy dissipated by ridging, q_r, has correlation coefficients, r, of 0.67 and 0.68 at 10 and 32 Hz, respectively. The energy dissipated by shearing, q_s, explains much less of the variance, with correlation coefficients of 0.36 and 0.37 at 10 and 32 Hz, respectively. Both coefficients vary greatly from one 20-day block to another. For completeness, p_ℓ is also used as a measure of energy dissipation to simulate noise. It does not do as well as q_r, except at times when q_s is better, because $p_\ell = q_r + q_s$ and both q_r and q_s are correlated somewhat. During Julian days 361 through 380, ridging explains very little of the noise, whereas shearing explains a larger amount. This is a rather quiet time, but one during which energy is dissipated in numerous high-frequency spikes. For Julian days 381 through 460, the correlation coefficient is consistently higher for noise simulated from q_r. However, during the period between Julian days 461 and 480, q_s is again greater than q_r, but for both the correlation coefficients are high. The threshold in simulated noise reduces the correlation when noise levels are low. Lag correlations were also determined. Maximum correlations appear at zero lag. Correlations are about as high at lag times of 3 h but not substantially higher. This is likely caused by the original filtering of motion and noise data to remove high-frequency input. To learn further how well simulated noise can explain observed noise, a regression analysis was performed. Multiple regressions of observed noise onto energy dissipated by ridging and shearing do not explain a more appreciable amount of the variance.

locations because they are caused by atmospheric pressure systems moving across the Beaufort Sea. One can expect, then, that many variables will rise and fall at roughly the same time.

The simulated noise is nearly always nonzero, while the observed noise drops to nearly zero at times. This threshold for the simulated noise is attributed to velocity inhomogeneities. These uncorrelated, random motions of individual ice floes dissipate energy in the model because of the dissipative nature of plasticity. An estimate of the size of this contribution may be made during two quiet periods, Julian days 411 through 421 and 451 through 461. The 10- and 32-Hz simulated noise levels from q_r have values on the order of 0.2×10^8 and 1.0×10^7 mW/m^2, respectively. The threshold levels for noise from q_s are about half these values.

On a few occasions, either the simulated or the observed noise curve indicates energy input but the other does not. Noise observed in the absence of a simulated noise signal can occur if it is generated by a process other than ridging. On the other hand, simulated noise can occur in the absence of observed noise if the model dissipates energy at a location too close to the sensor. The simulated noise is very sensitive to the location of energy dissipation when near the sensor, i.e., within about 100 km. Since the location of the dissipated energy can only be resolved to within about 50 km, this limits the accuracy to which the nearby noise can be simulated.

B. Correlation

A quantitative measure of comparison is obtained by determining the correlation between observed and simulated noise. Correlation coefficients are presented in Table II. The time series is broken into 20 day blocks to [illegible] if

data for the 10- and 32-Hz noise appear. The observed noise and the ice velocity data have been filtered to remove variations with a period shorter than one day. All data are sampled at synoptic time intervals. Simulated noise has been presented using both the energy dissipated in ridging, q_r, and the energy dissipated in shearing, q_s as energy dissipation sinks.

These time histories show, in a qualitative way, the ability of the model to simulate background noise. Intensities of the acoustic signals are presented on a linear scale. Observed noise is measured in units of square micropascals per hertz, $(\mu Pa)^2/Hz$. This is the power of the acoustic wave per unit area. The values for the simulated noise are given in milliwatts per square meter, mW/m^2. This scale is arbitrary because the signature function S(f) is not included in the calculation. Since it is a constant for each frequency band, a comparison may be made in the form shown. A linear regression is used to provide an estimate of the value of the signature function at each of the two frequencies.

A visual comparison of the observed and simulated noise from q_r is good. However, the comparison between observed and simulated noise from q_s is not as good. Both observed and simulated time histories are similar for the 10 and 32 Hz signals. The variations generally occur at the same times and have similar durations. Furthermore, the sizes of the larger events are comparable. This comparison is especially good during the most intense events (for example, between days 392 and 411 and days 438 and 443). Activity appears to rise at roughly 5-day intervals as storms pass through the Beaufort Sea. This relates to the energy input by the wind field. Previous estimates[12] of the energy input by winds and currents during the period under consideration here provide similar results. There is a strong correlation between wind at differen

of simulated noise require that the integrand in (25) be evaluated. We have assumed that the power dissipated is homogeneous within each triangle so that it may be removed from under the integral. The transmission loss remains to be integrated. A numerical integration scheme is chosen using values of the integrand at the midpoints of the sides (denoted by subscripts a,b and c) so that

$$\int_A T(|\underset{\sim}{x}-\underset{\sim}{y}|,s,f)\,da = \frac{A}{3}\left[T(|\underset{\sim}{R}_a|,s,f) + T(|\underset{\sim}{R}_b|,s,f) + T(|\underset{\sim}{R}_c|,s,f)\right] \quad . \qquad (26)$$

This is a simple formula that is accurate to the second order.[21]

A higher order integration formula could have been used to integrate the transmission loss contribution within each triangle. Such accuracy, however, would ignore the fact that all variations of q have been neglected and, therefore, would not provide increased accuracy in the simulated noise. Also, the simplest formula expressed in terms of values at the corners is troublesome when considering those triangles at whose corners the noise is being simulated because the transmission loss is not appropriate for propagation ranges less than 37 km (20 nautical miles).

III. RESULTS

Background noise simulated using the model is compared with observed noise for one site in the Beaufort Sea during a 4-month period in the winter of 1975-76. A time history of data is presented. Statistical correlations and linear regressions are used to quantify the comparison.

A. Time history

A direct comparison between observed and simulated time histories of noise at telephone site number 11 (Figure 2) is presented in Figures 3 and 4. A

When the array was deployed, the Beaufort Sea region was subdivided into 38 triangles as shown in Figure 2 (solid lines). After Julian day 421, buoy number 16 moved rapidly into the Chukchi Sea, and these triangles became too distorted for meaningful simulations; the five triangles surrounding the buoy collapsed into three triangles (dashed lines).

The integral in Eq. (24) sums noise signals from surrounding locations. It may by evaluated as a sum of integrals over the set of triangles. The advantage of introducing the triangles is that the energy sink q may be estimated simply in each smaller triangular region. Since q is calculated as the product of stress and stretching, both variables must be calculated in each triangle. Average stretching is estimated directly from velocities of buoys located at each corner. Stress is estimated by solving the constitutive law by integrating the stretching history. The product then gives the desired energy dissipation.

The motions of three buoys are used to determine the velocity gradient, $\underset{\sim}{L} = \underset{\sim}{\nabla} \underset{\sim}{v}$. The average may be found by using the Green-Gauss theorem to express the integral as a line integral and then assuming linear variation of velocity along the boundary. The relationship becomes

$$A \underset{\sim}{L} = \int_S \underset{\sim}{v} \otimes \underset{\sim}{n} \, d\ell \tag{25}$$

where $\underset{\sim}{L}$ is the gradient of the average ice velocity, $\underset{\sim}{v}$, over the region R bounded by the curve S.

The stress history is obtained from the elastic-plastic constitutive law while assuming homogeneous stretching within each triangle. Equations (1) through (5) are integrated numerically using a difference scheme[20] as part of the numerical scheme to solve the sea ice dynamics model. Actual estimates

Therefore, if we are able to estimate the signature function, S(f), for a selected noise-making process, then the noise that will be observed at a site $\underline{x}$ from the process will be given by (24) in terms of the energy dissipated at all locations and times. We have included the time variable t to show explicitly how temporal energy variations in energy dissipation cause time variations in noise generation.

II. SIMULATION TECHNIQUE

During the AIDJEX main experiment (the winter of 1975-76), an array of buoys and omnidirectional hydrophones was deployed in the Beaufort Sea.[18,19] The hydrophones were suspended at a depth of 100 ft below the top of the ice. The pressure measurements were converted to acoustic intensities using a power meter. They were band-pass filtered into one-third octave bands centered on 3.2, 10, 32 and 1000 Hz (in one case, 100 Hz replaced 32 Hz). Signals were averaged over 45 s and sampled at 3-hr synoptic time intervals. The 3.2-Hz data were contaminated by noise from cable strum. The other data are felt to be adequate, although sampling frequencies are too low.

Figure 2 shows the spatial distribution of the AIDJEX sensors on Julian day 381 (January 16, 1976). The data are adequate to estimate dissipation by ridging and to compare simulated noise with the levels observed at one hydrophone site, site number 11. To account for all noise received at a site, sound waves propagating to it from all directions must be included in the model. This requires that ice motion data be available all around the site, which limited study to site number 11, the only hydrophone site in the central buoy array.

As the acoustic signal propagates from the source, it undergoes geometrical dispersion and dispersion due to reflections off the sea floor and the underside of the ice cover and to gradients in the water column. An empirical model has been presented for long-range, low-frequency (i.e., below 100 Hz), deep-water (greater than 1000 m) transmission loss, TL, in the Arctic.[17] The equation is

$$TL = a + 10 \log R + bf + csR + dfsR \tag{22}$$

where

R is the range in kilometers,

s is the standard deviation of ice depth in meters, and

f is the frequency in hertz.

The constants a, b, c, and d are given in Table I as a function of path length.

The loss function T is related to transmission loss TL by

$$T = 10^{-TL/10} \quad . \tag{23}$$

Figure 1 presents the loss function for waves with frequencies of 3.2, 10, 32, and 100 Hz. The transmission loss law given in Eq. (22) is evaluated for frequencies from 3.2 to 100 Hz. Each curve has been normalized to unity at a range of 50 km. Within this range the relative intensity is assumed constant. This assumption is compatible with the restriction that the law is valid only for propagation paths in excess of 37 km (20 nautical miles). It will be seen that this assumption is also comparable with the resolution of ice motion data used in this study to simulate noise.

If the assumed relationship between the source level noise and dissipated energy is substituted, we find that

$$N(\underset{\sim}{x},f,t) = S(t) \int_A q(\underset{\sim}{y},t)\, T(|\underset{\sim}{x}-\underset{\sim}{y}|,s,f)\, da \quad . \tag{24}$$

It is worth noting that q and therefore N_s depend explicitly on the horizontal position $\underset{\sim}{x}$. We do not, however, attempt to describe the dependence on depth, being content at this time with a two-dimensional theory, because data are available at only one depth in our data set. Other variables such as ice conditions affect only q and do not appear in any other ways in the noise source definition.

C. Simulated noise

At each location at which noise is generated it is necessary to sum source level noise contributions from all noise generation mechanisms. If it is assumed that there are enough sources that the acoustic signals are uncorrelated, then waves must cause interference, but intensities may still be added together linearly. This is a consequence of the fact that intensity is the square of the pressure in an acoustic signal and that uncorrelated acoustic waves are included in a mean square sense.

The intensity of noise at any site is obtained by adding together the contributions from all surrounding sources. This is accomplished by integrating over the region of interest, A, with the integrand being the propagated noise intensity per unit area. Thus, we write

$$N_s(\underset{\sim}{x},f) = \int_A N_s(\underset{\sim}{y},f)\, T(|\underset{\sim}{x}-\underset{\sim}{y}|,s,f)\, da \qquad (21)$$

where $\underset{\sim}{x}$ is the site at which the noise is to be predicted or observed, $\underset{\sim}{y}$ is the integrand in the generic location of each point in the region, $|\underset{\sim}{x}-\underset{\sim}{y}|$ is the range of the propagation path and T is a loss function (the relative intensity of the acoustic wave after propagating from $\underset{\sim}{y}$ to $\underset{\sim}{x}$).

B. Noise source intensity

Consider the key assumption that small-scale energy sinks associated with large-scale ridging deformations are related to the source level intensity of acoustic signals generated by these mechanisms. This assumption is attractive for two reasons. First, both quantities are measures of energy and thus this relationship is more physically meaningful than a relationship between energy and another variable such as strain, stress, ice velocity, wind speed or air stress. Second, several limiting cases are identified where the energy relationship is sensible and other relationships are not. These include situations in which

(a) Internal ice stresses are large, but not large enough to cause plastic deformation; in this case, no energy is dissipated by ridging and no noise is expected.

(b) Strains are large but stresses are small because of a large fraction of open water; in this case, only a little energy is dissipated and little noise is expected.

The simplest assumption that can be made is that the intensity of each noise source is linear in the rate of dissipation of energy by that mechanism. Each mechanism is expected to produce noise in a different range of frequencies. Therefore, a scalar signature function relating the power dissipated, q, to the noise source level is introduced. This signature function, S(f), must depend on frequency. Each mechanism will have its own signature or dependence on frequency. If the amplitude of the noise source intensity generated by the mechanism is $N_s(f)$, then the noise source level is given for a typical process as

$$N_s(\underline{x},f) = S(f)\, q(\underline{x}) \qquad (20)$$

In addition to defining strength, relating dissipative stress power to energy dissipated by small-scale sinks also introduces a constraint between the yield surface shape and the coefficient that controls the amount of open water formed in compression and shearing.

The energy dissipated in shearing, q_s, is assumed to depend linearly on the rate of permanent stretching and on ice strength[9]:

$$q_s = D_p \alpha_s p^* \tag{19}$$

where the coefficient $\alpha_s(\theta)$ is determined from the coefficient α_r and the yield surface.

This sink has not been analyzed by considering a small-scale mechanism but has been introduced as a residual in the large-scale model energy budget. The shear energy sink describes energy dissipated without redistribution of ice. It is possible to think of this term as representative of energy dissipated in building shear ridges. Since shear ridges are narrow features, they do not affect the thickness distribution significantly. However, the size of the shear energy term is determined without consideration of any specific mechanism. When the shear sink is included, large-scale strength still satisfies (19), but there is no longer a constraint between the yield surface shape and the formation of open water. Instead, both variables are specified independently using observations and results of simulations of ice behavior.

Integration of the thickness distribution equation requires that an initial condition be described. This quantity can have a strong impact on the ice simulation because it affects stress. We have chosen an initial thickness distribution observed by investigators on the USS Gurnard during a cruise under the Beaufort Sea ice during April 1970.

where ρ is the density of the ice and ρ_w that of the water. If the redistribution function (6) is substituted, then

$$q_p = D_p \alpha_r p_p^* \tag{11}$$

where

$$p_p^* = c_p \int_0^\infty h^2 \frac{\partial W_r}{\partial h} dh \quad . \tag{12}$$

The power dissipated by friction, q_f, has the same functional form as gravitational potential energy changes and may be written as

$$q_f = D_p \alpha_r p_f^* \tag{13}$$

where

$$p_f^* = c_f \int_0^\infty \frac{h^2 a(h)}{1-(1/k)} dh \tag{14}$$

and

$$c_f = \frac{\mu'(\rho_w - \rho)g}{2 \tan \phi'} \left[\frac{\rho(k-1)}{\rho_w}\right]^2 \quad . \tag{15}$$

Here, a(h) is the fraction of ice present in a category that participates in ridging, k is a constant that determines the ratio of final to original thickness during the ridging process and it defines the fall angle of the ridge sail and keel, μ' is the coefficient of sliding friction of ice, and ϕ' is the angle of friction of the blocks of ice in the ridge. When realistic constant are used, friction accounts for over 80% of the energy dissipated. When these two energy sinks are combined, the large-scale strength becomes

$$p^* = p_p^* + p_f^* \tag{16}$$

or

$$p^* = c^* \int_0^\infty h^2 a(h) dh \tag{17}$$

and

$$c^* = \frac{1}{2} \rho g k \left[1 + \frac{\mu'}{\tan \phi'} \frac{\rho}{\rho_w} (k-1)\right] \tag{18}$$

account, the noise propagating from all sources to any site may then be simulated. This model of background noise is based on the fundamental principles of acoustic propagation.

Observed background noise in the Beaufort Sea during the AIDJEX field experiment in 1975-76 is used to test the model. Low-frequency noise signals (10 and 32 Hz) are compared with the simulated noise. Time histories of observed and simulated noise compare well in frequency, duration and magnitude. The model simulates 46% of the variance of observed noise during a 120-day test period (the correlation coefficient is 0.67). The comparison is broken into 20-day intervals to determine variations in time. During several of these 20-day intervals, the model has a correlation of over 0.80, explaining over 64% of the variance. When potential error sources are considered, it is found that much more of the variance could be explained by the model if several error sources could be reduced.

This comparison is good enough to warrant further study and testing of this new concept. First, however, data sets must be obtained in other regions and at other times, since various noise-making processes will contribute different amounts of noise in different areas, such as at an ice edge. Also, ice motion, wind and current data must be used in a complete ice dynamics simulation model to avoid contamination by velocity inhomogeneities. A limited amount of data exists for areas other than the Beaufort Sea, and recent field experiments, such as FRAM[23] and MIZEX,[24] will provide more data. Further testing with these additional data will help determine the range of applicability of the concept that energy dissipated by the ice cover is a useful measure of the sources of ambient noise

The statistical approach presented here ignores the physical causes of noise generation. To this end, this paper has focused on showing that one of these, namely the power dissipated by ridging, is highly correlated with background noise. Since there are many sources of noise, we cannot expect a perfect correlation with only one source. Instead, the simulation model can be used to verify qualitatively the contribution of each noise-making process and then to determine how much of the observed noise is accounted for by each process.

ACKNOWLEDGEMENT

I thank K. L. Hammond for outstanding technical writing and editing help in preparing this paper. This work was funded by the Office of Naval Research Arctic Program Office (contract number N00014-82-C-0002). I thank Dr. Leonard Johnson, Director, for his support of this work.

REFERENCES

[1]O. Diachok, "Arctic hydroacoustics," Cold Regions Science and Technology 2, 299-321 (1980).

[2]C. R. Greene, "Arctic Ocean ambient noise," J. Acoust. Soc. Am. 36, 1218-1220 (1964).

[3]C. R. Greene and B. M. Buck, "The influence of atmospheric pressure gradient on under-ice ambient noise," J. Underwater Acoust. 28(4), (1977).

[4]R. H. Mellen and H. W. Marsh, "Underwater sound in the Arctic Ocean," Report MED-65-1002 (U.S. Navy Underwater Sound Laboratory, New London, CN, 1965).

[5]J. H. Ganton and A. R. Milne, "Temperature and wind-dependent ambient noise under midwinter pack ice," J. Acoust. Soc. Am. 38, 406-411 (1965).

[6]A. R. Milne, "Statistical description of noise under shore-fast sea ice in winter," J. Acoust. Soc. Am. 39, 1174-1182 (1966).

[7]The Arctic Ice Dynamics Joint Experiment (AIDJEX) was a program sponsored jointly by the National Science Foundation and the Office of Naval Research during 1970-79 to study ice dynamics in the Alaskan Beaufort Sea by deploying buoys to collect data and developing models to simulate the dynamic behavior of sea ice.

[8]M. D. Coon, "A review of AIDJEX modeling," in Sea Ice Processes and Models, edited by R. S. Pritchard (University of Washington Press, Seattle, WA, 1980), pp. 12-27.

[9]R. S. Pritchard, "Mechanical behavior of pack ice," in Mechanics of Structured Media, edited by A. P. S. Selvadurai (Elsevier, Amsterdam, 1981), pp. 371-405.

[10]M. D. Coon and R. S. Pritchard, "Mechanical energy considerations in sea ice dynamics," J. Glaciology 24(90), 377-389 (1979).

[11] R. S. Pritchard, M. D. Coon, and D. R. Thomas, "Modeling the mechanical energy budget of the Beaufort Sea ice cover," Flow Research Report No. 137R (Flow Industries, Inc., Kent, WA, 1979), 51 pp.

[12] D. R. Thomas and R. S. Pritchard, "Beaufort Sea ice mechanical energy budget 1975-76," Flow Research Report No. 165 (Flow Industries, Inc., Kent, WA, 1980), 37 pp.

[13] R. S. Pritchard, "An elastic-plastic constitutive law for sea ice dynamics," J. Appl. Mech. 42(2), 379-384 (1975).

[14] A. S. Thorndike, D. A. Rothrock, G. A. Maykut, and R. Colony, "The thickness distribution of sea ice," J. Geophys. Res. 80(33), 4501-4513 (1975).

[15] R. R. Parmerter and M. D. Coon, "Model of pressure ridge formation in sea ice," J. Geophys. Res. 77(33), 6565-6575 (1972).

[16] D. A. Rothrock, "The energetics of the plastic deformation of pack ice by ridging," J. Geophys. Res. 80(33), 4514-4519 (1975).

[17] B. M. Buck, "Some preliminary considerations of the relationships of Arctic acoustic ambient noise, low frequency propagation, ice movement and ice roughness," (Polar Research Laboratory, Inc., Santa Barbara, CA, 1981).

[18] C. R. Greene and B. M. Buck, "Arctic noise measurement experiment using Nimbus-6 data buoys," J. Underwater Acoust. 27(4), (1977).

[19] P. Burke and B. M. Buck, "The Synrams ice station," in Proc. IEEE Ocean 1975 Conference, 413-417 (1975).

[20] R. S. Pritchard and R. Colony, "A difference scheme for the AIDJEX sea ice model," in Numerical Methods in Geomechanics (American Society of Civil Engineers, New York, 1976), Vol. II, pp. 1194-1209

[21] K. H. Huebner, The Finite Element Method for Engineers (John Wiley, New York,

[22]A. S. Thorndike and R. Colony, "Estimating the deformation of sea ice," in POAC77, edited by D. B. Muggeridge (Memorial University of Newfoundland, St. John's, Newfoundland, 1977), pp. 506-517.

[23]A. Baggeroer and I. Dyer, "FRAM 2 in the Eastern Arctic," Eos Trans. AGU 63(14), (1982).

[24]M. G. McPhee, "Greenland Sea ice/ocean margin," Eos Trans. AGU 64(9), 82-83 (1983).

FIGURE 1. Relative intensity of acoustic waves. The transmission loss function is given for long-range, low-frequency propagation over deep water.

FIGURE 2. Spatial distribution of AIDJEX sensors in the Beaufort Sea on Julian day 381 (January 16, 1976).

FIGURE 3. Comparison between observed background and simulated noise by ridging for 120 days in winter 1975-76. Data are presented for the one-third octave band centered around 10 Hz. Sound intensity is presented. Simulated sound intensity is nondimensional with an arbitrary scale because the signature function S(f) is unknown.

FIGURE 4. Comparison between observed background and simulated noise by ridging for 120 days in winter 1975-76. Data are presented for one-third octave bands centered around 32 Hz. Sound intensity is presented. Simulated sound intensity is nondimensional with an arbitrary scale because the signature function S(f) is unknown.

FIGURE 5. Observed noise and simulated noise from energy dissipated by ridging, q_r, at 10 Hz.

FIGURE 6. Observed noise and simulated noise from energy dissipated by ridging, q_r, at 32 Hz.

TABLE I. Transmission loss law constants.

Path Length	Less than 185 km (100 nautical miles)	Greater than 185 km (100 nautical miles)
Constant		
a	69.3	63.2
b	0.07	0.03
c	-0.00081	0.035
d	0.00026	0.00059

TABLE II. Correlation between observed background noise intensity and noise intensity simulated by power dissipated by sea ice cover in the central Beaufort Sea during the AIDJEX main experiment (winter 1975-76). All data were filtered to remove frequency content higher than 1 cycle per day and then sampled at 3-hr intervals.

Date (Julian day)	Correlation coefficient, r					
	10 Hz			32 Hz		
	p_ℓ	q_r	q_s	p_ℓ	q_r	q_s
361-380	0.36	0.28	0.48	0.21	0.09	0.50
381-400	0.62	0.68	0.44	0.33	0.46	0.12
401-420	0.75	0.80	0.47	0.88	0.89	0.55
421-440	0.66	0.74	0.25	0.77	0.78	0.30
441-460	0.85	0.86	0.25	0.89	0.90	0.76
461-480	0.87	0.76	0.83	0.78	0.61	0.82
361-	0.63	0.67	0.36	0.66	0.68	0.37

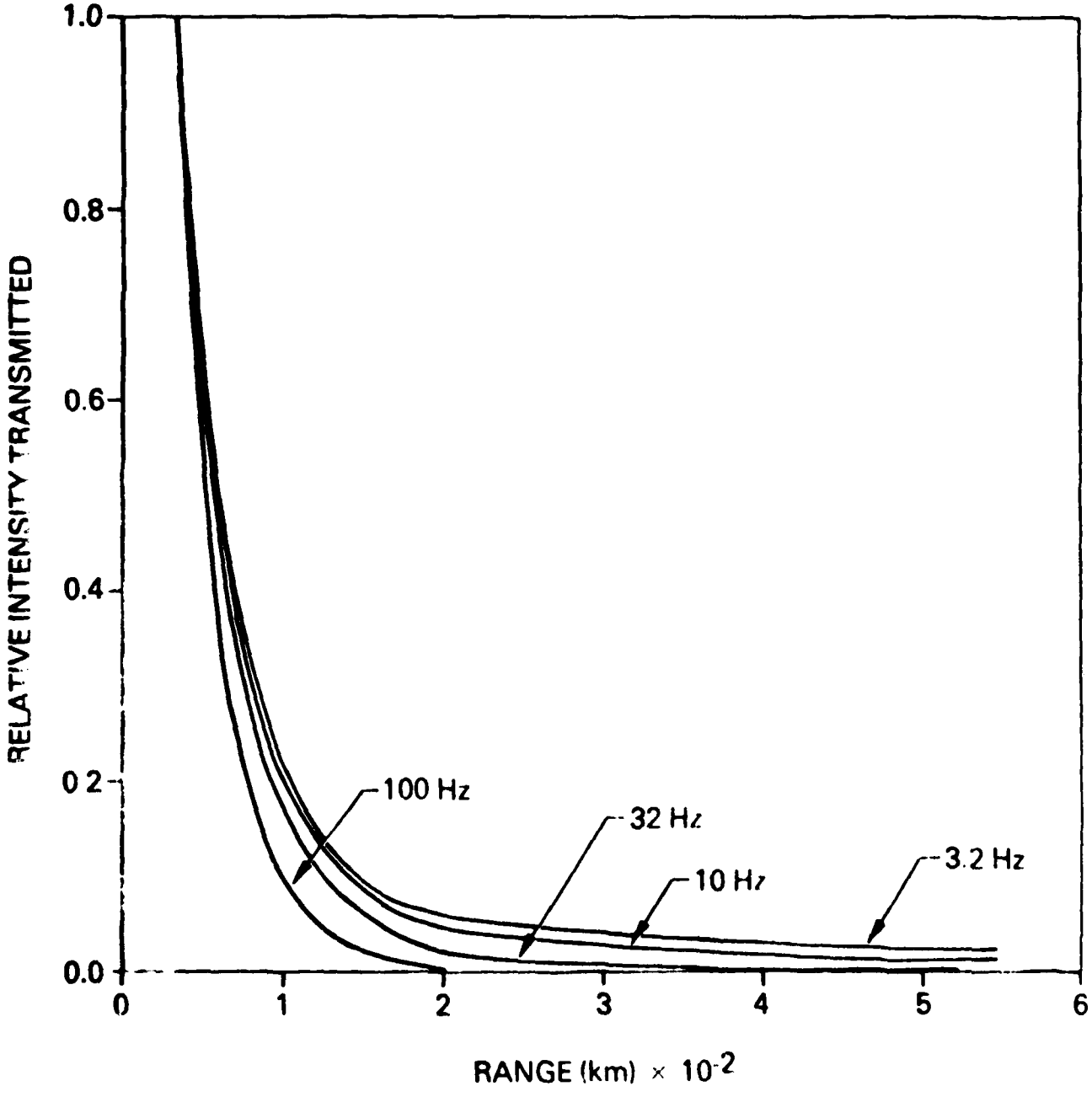

Relative Intensity of Acoustic Waves

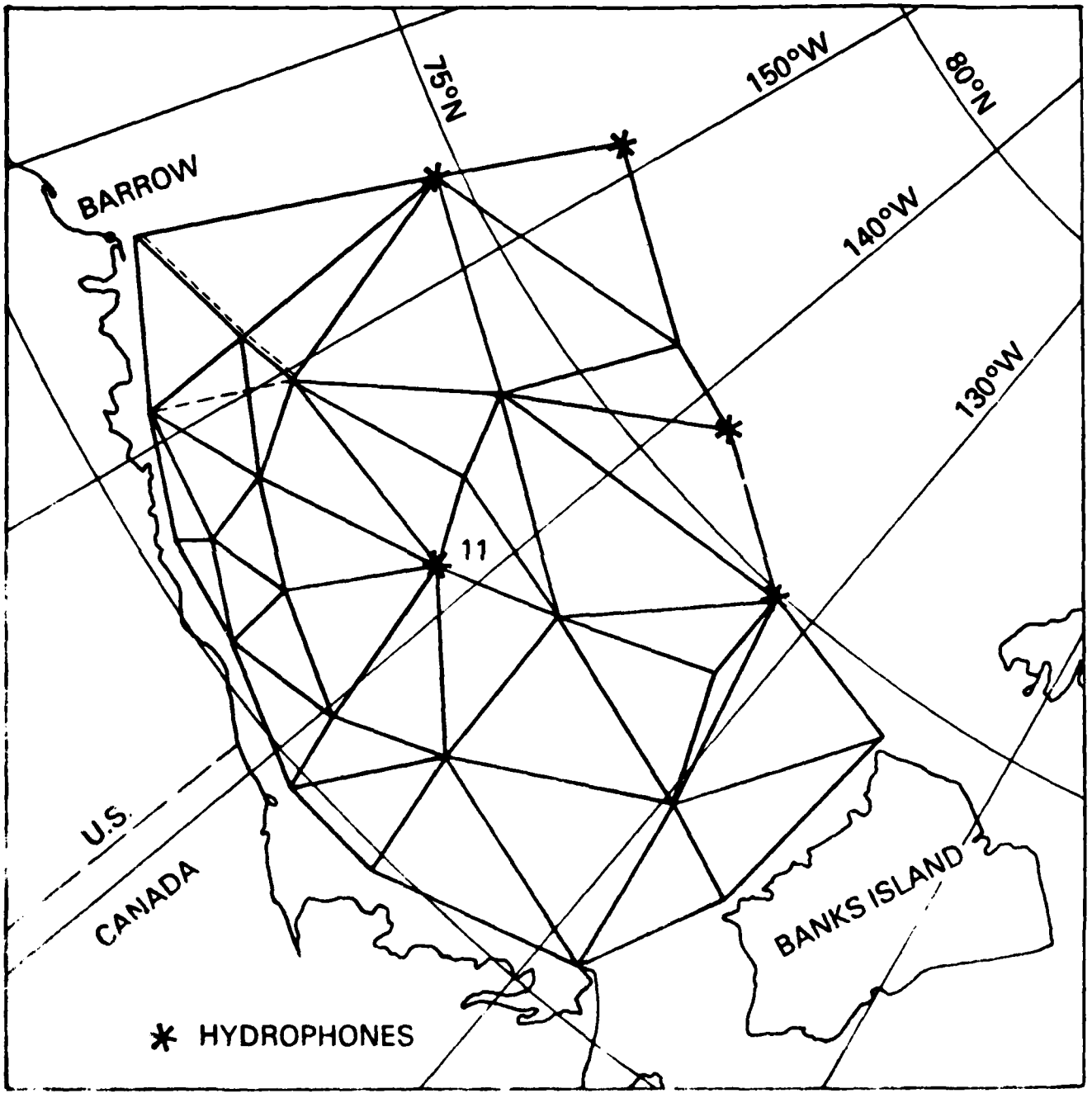

Figure 2. Spatial Distribution of AIDJEX Sensors in the Beaufort Sea on Julian day 381 (January 16, 1976).

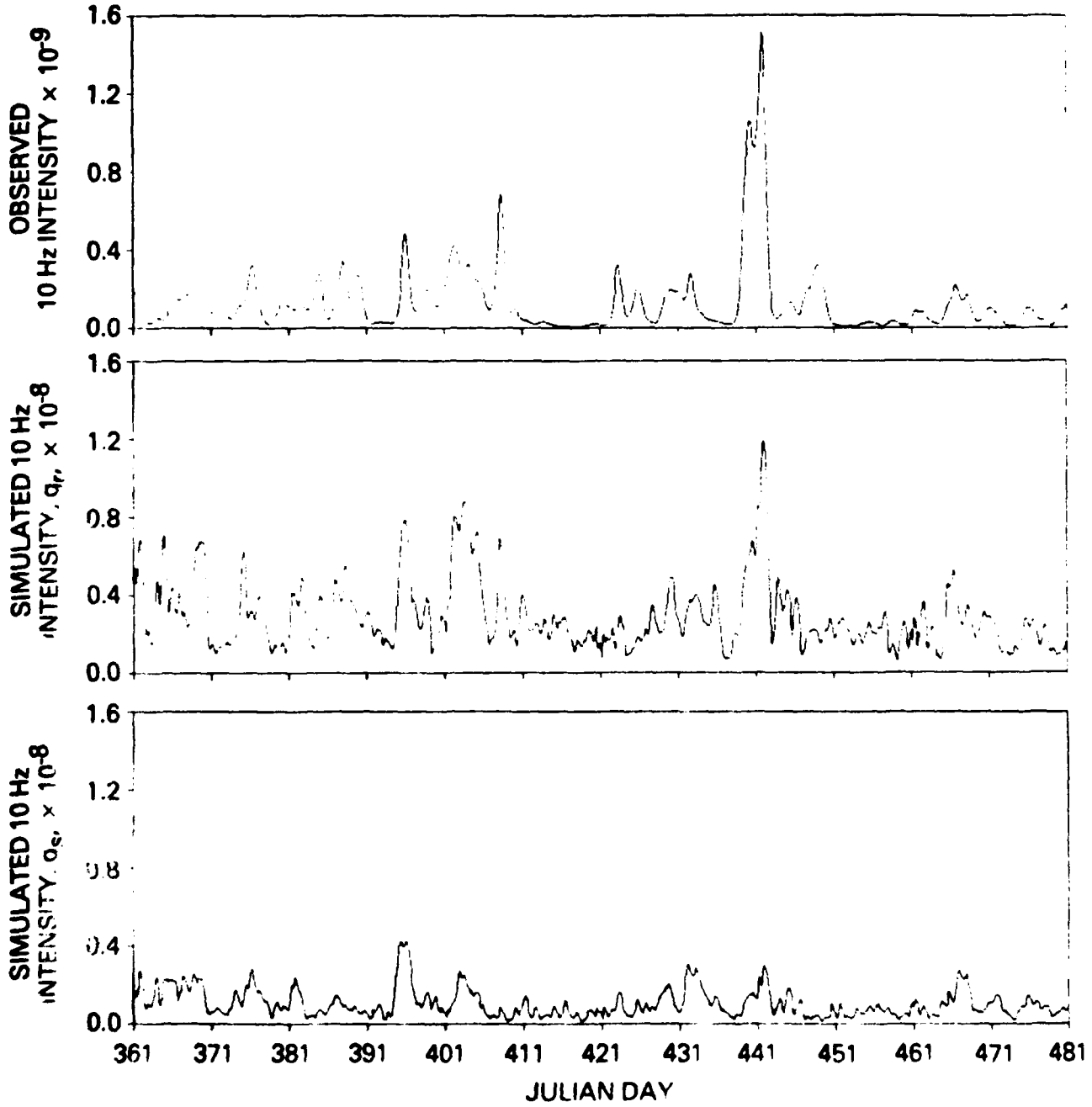

Figure 3. Comparison Between Observed Background and Simulated Noise by Ridging for 120 Days in Winter 1975-76.

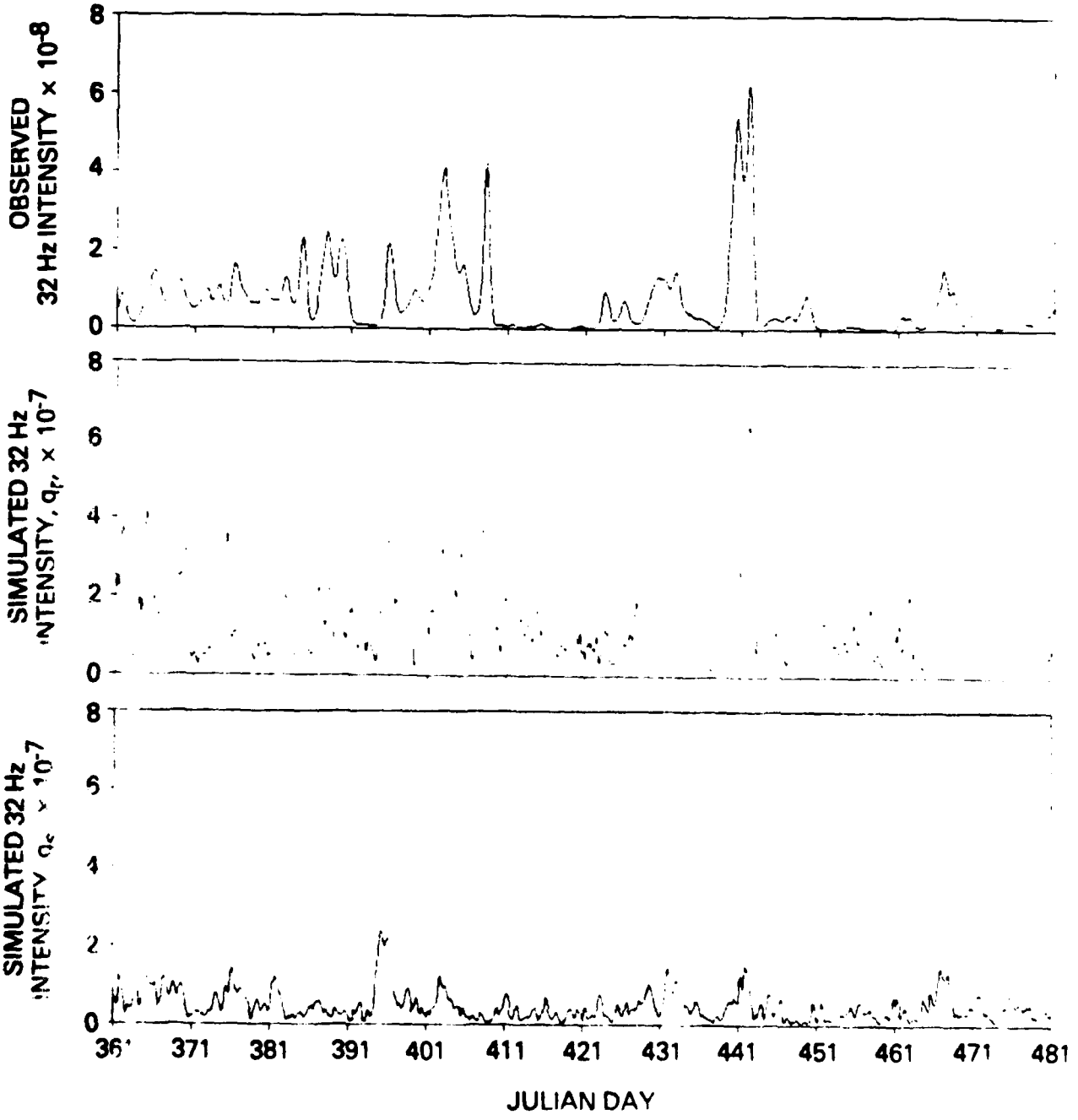

Figure 4. Comparison Between Observed Background and Simulated Noise by Ridging for 120 Days in Winter 1975-76.

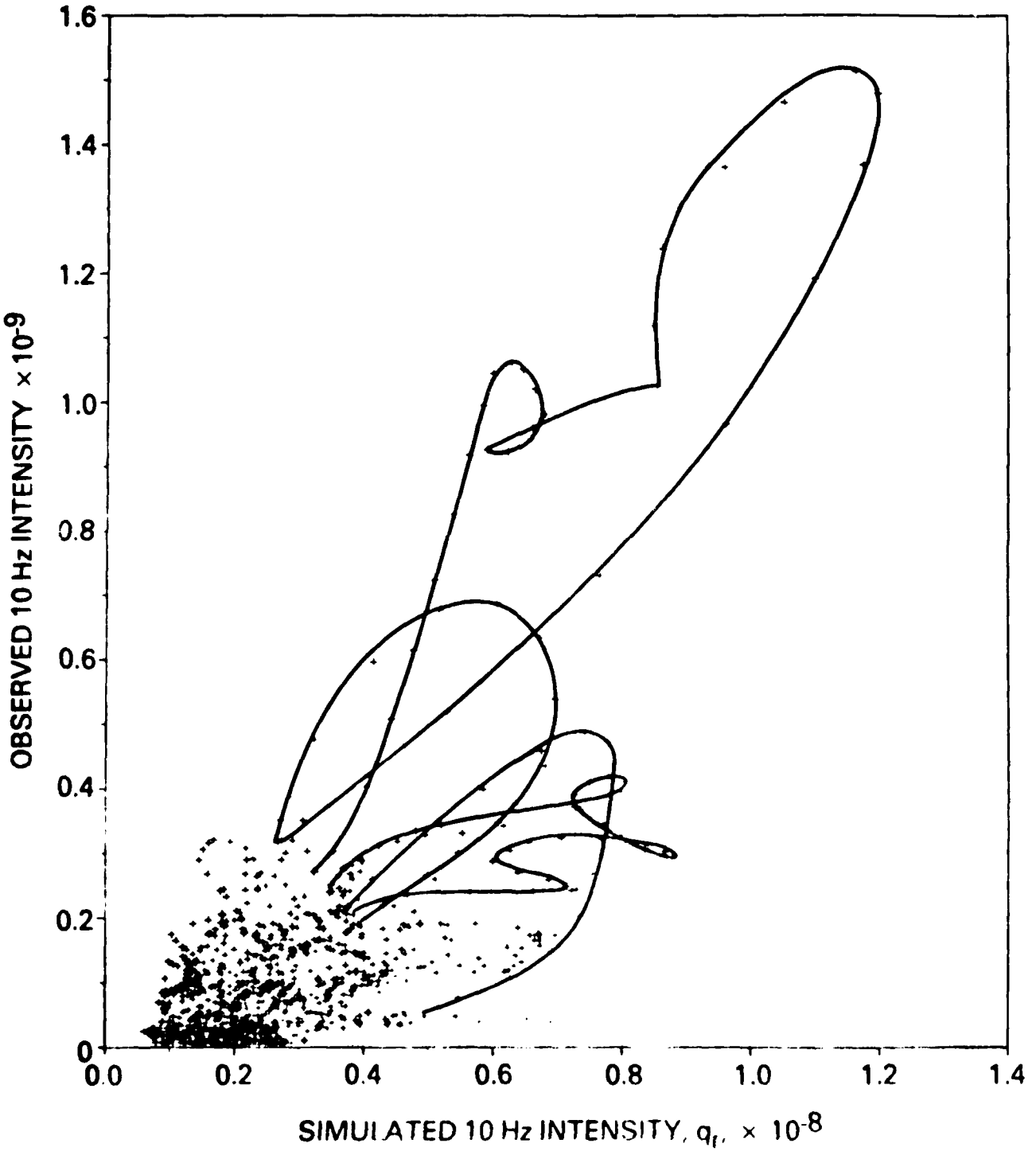

Figure 5. Observed Noise and Simulated Noise Power Distribution by Ridging, q_t, at 10 Hz.

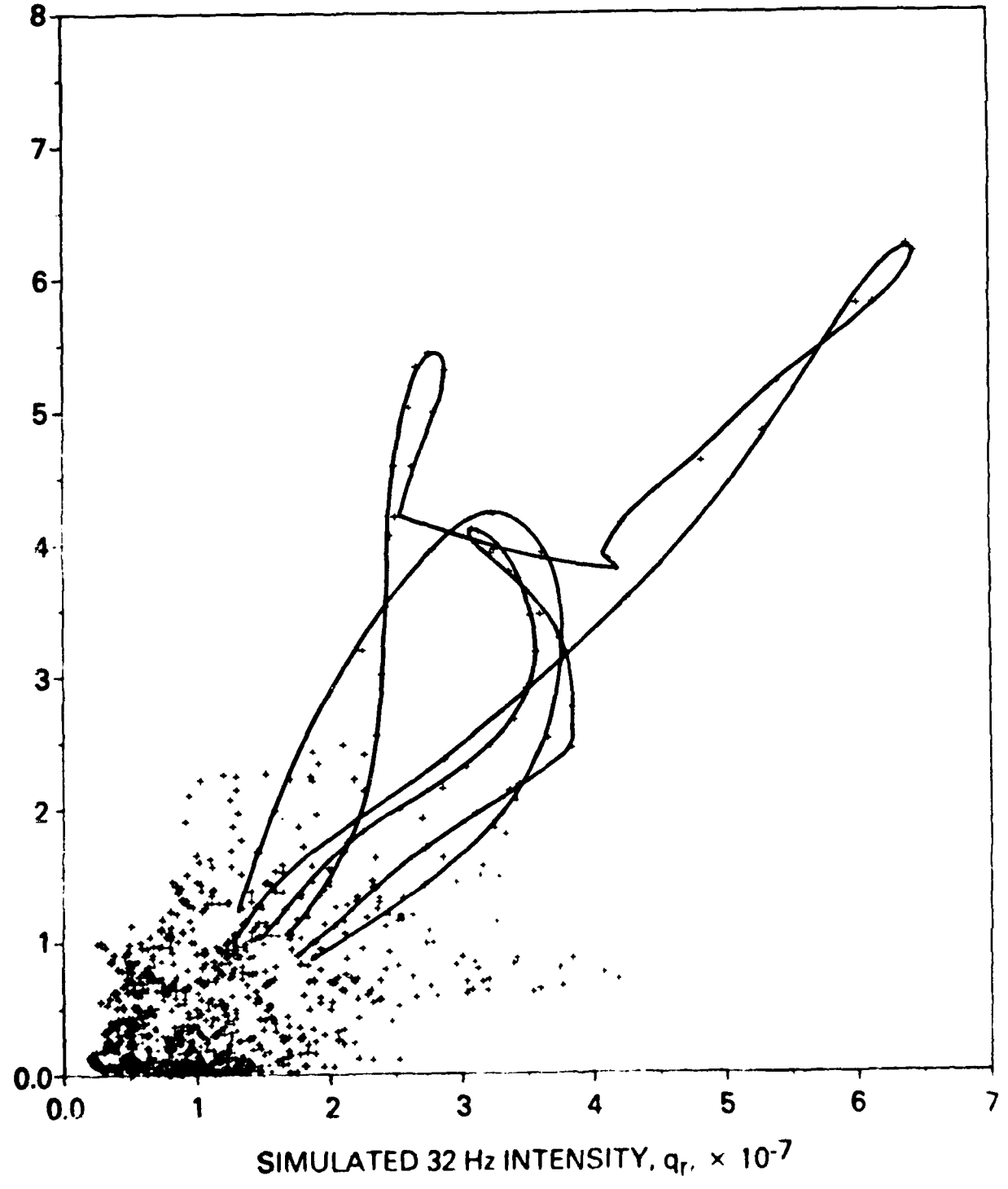

Figure 6. Observed Noise and Simulated Noise from Energy Integrated in Ridgline, q_r, at 32 Hz

END

FILMED

10-85

DTIC